Potential-field modelling of the prospective Chibougamau area (NE Abitibi subprovince, Quebec) using geological, geophysical and petrophysical constraints

Maleki, A.[1], Smith, R. S.[1], Eshaghi, E.[1, 2, 4], Mathieu, L.[3], Snyder, D.[1], Naghizadeh, M.[1]

[1] Mineral Exploration Research Centre, Harquail School of Earth Sciences, Laurentian University, 935 Ramsey Lake Road, Sudbury, ON P3E 2C6

[2] ExploreGeo, Wangara, WA, Australia

[3] UQAC institutional Chair on Archean metallogenic processes, Centre d'études sur les Ressources minérales (CERM), Département des Sciences appliquées, Université du Québec à Chicoutimi (UQAC), 555 boul. de l'université, Chicoutimi, G7H 2B1 QC, Canada

[4] School of Natural Sciences (Earth Sciences) and ARC Centre of Excellence in Ore Deposits (CODES), University of Tasmania, Private Bag 79, Hobart, TAS, Australia, 7001

Maleki, A.: email: malekiamir3034@gmail.com

Smith, R. S.: email: RSSmith@laurentian.ca

Eshaghi, E.: email: eshaghi.es@gmail.com

Mathieu, L.: email: Lucie1_Mathieu@uqac.ca

Snyder, D.: email: dbsnyder1867@gmail.com

Naghizadeh, M.: email: mnaghizadeh@laurentian.ca

Corresponding author: Amir Maleki, call: 6478304930, (malekiamir3034@gmail.com)

Contribution number: MERC-ME-2019-225

Abstract:

This contribution focusses on obtaining a better understanding of the subsurface geology of the Chibougamau area, in the NE of the Abitibi greenstone belt (Superior craton), using geophysical data collected along a 128 km long traverse with a rough SW-NE orientation. We have constructed two-dimensional (2D) models of the study area that are consistent with newly collected gravity data and high-resolution magnetic datasets. The initial models were constrained at depth by an interpretation of a new seismic section and at surface by the bedrock geology and known geometry of lithological units. The attributes of the model were constrained using petrophysical measurements so that the final model is compatible with all available geological and geophysical data.

The potential-field data modelling resolved the geometry of plutons and magnetic bodies which are transparent on seismic sections. The new model is consistent with the known structural geology, such as open folding, and provides an improvement in estimating the size, shape, and depth of the Barlow and Chibougamau plutons. The Chibougamau pluton is known to be associated with Cu-Au magmatic-hydrothermal mineralisation and, as the volume and geometry of intrusive bodies is paramount to the exploration of such mineralisation, the modelling presented here provides a scientific foundation to exploration models focused on such mineralisation.

Key words: Geophysics, Potential-field modelling, 2.5-D modelling, Geological modelling, Geological, seismic and petrophysical constraints, Gravity and Magnetic

1. Introduction

The Metal Earth (ME) project aims to better understand the differences between greenstone belts in the Abitibi and Wabigoon belts of the Superior craton of Canada that are well endowed with gold and base metal mineralisation from those that are less endowed, in the hope that exploration can focus on the more prospective belts, and locations within there belts where there might be deposits that have not been discovered. This new understanding is intended to come through a combination of geological mapping (lithological and structural), geochemical and geochronological studies, mineral deposits studies, mantle studies and deep probing geophysics.

The seismic data collected along the 128-km long Chibougamau profile as part of the Metal Earth project allows the characterization of shallow-dipping reflective features and a number of these have been identified at depths below 5 km. Where it appears that a significant number of these reflectors terminate, major faults have been interpreted. However, the upper crust above 5 to 10 km contains very few seismic reflections, so it is termed seismically “transparent”. The lack of seismic features is most likely due to the steep dips of the geological interfaces, so seismic energy is not reflected back to the surface, or it might be due to an insufficient contrast in the seismic properties between different lithologies. Our aim is to use the gravity and magnetic data to provide information about the geology in the upper crust. In particular, this study aims at defining the geometries of the intrusive bodies, as these can generate magmatic-hydrothermal systems. The fluids associated with these systems can transport the metals and result in mineral deposits that are of interest to explorationists. A better understanding of the relationship of the plutons to mineral deposits will help to define the character of the well-endowed areas that are of interest to the Metal Earth project. We are also interested in detecting lithological contacts and major fault zones that are transparent in the seismic section. These upper-crustal structures could then be extrapolated to

70 greater depth and associated with those evident on other geophysical data (magnetotelluric and
71 seismic). A better characterization of the subsurface geometry will also be useful in future studies
72 looking to understand the tectonic history of the area.

73 One of the challenges in potential-field data modelling is the concept of non-uniqueness, which
74 means that an infinite number of models can match the same observed geophysical data. A way to
75 mitigate the impact of non-uniqueness is to constrain the model with complementary data. In this
76 study, a set of constraints were used to construct the initial model and were also applied during
77 modelling to ensure that the final results are realistic. These constraints include bedrock geology
78 mapped at surface, existing geological sections, the interpreted seismic section and petrophysical
79 properties measurements. These data were compiled from previous studies. In the following four
80 sections, we briefly introduce the data that provide the constraints, any conclusions that were
81 drawn from these data and explain how they are relevant to the potential-field modelling described
82 in the latter part of this study.

83 **2. Compiled geological data**

84 The Chibougamau (Quebec) area is located in the NE corner of the neoarchean Abitibi greenstone
85 belt, the southern part of the Superior craton (Figure 1, inset). The study area is in contact with the
86 Opatica subprovince (greenstone and plutonic belts) to the north and the Grenville orogeny to the
87 east, metamorphosed during the Grenville orogeny occurring at ~1.1 Ga (Baker, 1980). The
88 Chibougamau area is the easternmost part of the 430 km long, E-W-striking Matagami-
89 Chibougamau greenstone belt (Wynne-Edwards 1972; Rivers and Chown 1986), and this belt has
90 a consistent structure over its whole length according to seismic reflection profiling (Mathieu et
91 al. 2020). This belt was mostly metamorphosed to greenschist facies, as are most supracrustal
92 rocks of the Abitibi greenstone belt (Faure 2015, Jolly 1974), except near intrusions (contact

93 metamorphism) and close to the contact with the Opatica subprovince to the north (where
94 amphibolite-grade metamorphism occurs).

95 The volcano-sedimentary assemblage of the Chibougamau area is mostly comprised of the ca.
96 >2730 Ma to 2710 Ma Roy Group, which sits on ca. 2790-2760 Ma volcanic units (Chrissie and
97 Des Vents Formations). The Roy Group is overlain by the sedimentary units of the Opémisca
98 Group. The Roy Group consists of volcanic cycle 1, which is dominated by mafic lava flows, and
99 volcanic cycle 2, which consists of mafic to felsic lava flows and pyroclastic rocks (Allard 1976;
100 Gobeil and Racicot 1983; Allard and Gobeil 1984; Daigneault and Allard 1987; Leclerc et al 2017).
101 In the study area, stratigraphic interpretation has recently been modified using new geochemical
102 and geochronological data (Leclerc et al. 2017) and, in this study, no reference will be made to
103 former stratigraphic interpretation (e.g., the former Gilman Formation).

104 Volcanic cycle 1 of the Roy Group consists of the undated Obatogamau and ca. 2730-2726 Ma
105 Waconichi Formations (Caty 1975; Daigneault and Allard 1990; Mortensen 1993; Leclerc et al.
106 2017). The Obatogamau Formation is a 3-4 km thick pile of feldspar megacrysts-bearing basaltic
107 to andesitic lava flows, which is conformably overlain by the ~800 m thick Waconichi Formation.
108 This latter formation consists of felsic volcanic rocks and contains several massive sulfide and
109 exhalative units such as the Lac Sauvage Iron Formation (thinly bedded siderite, pyrite, chert, and
110 iron oxides) (Henry and Allard 1979). The Obatogamau and Waconichi Formations are intruded
111 by the Doré Lake Complex, a thick anorthosite-dominated layered intrusion with vanadiferous
112 magnetite-rich upper units (Polat et al. 2018, Allard 1976, Mathieu 2018). Volcanic cycle 2 is
113 comprised of the Bruneau, Blondeau and Bordeleau Formations. The Bruneau Formation consists
114 of ca. 2724 Ma mafic to intermediate lava flows (3-4 km thick) (Leclerc et al. 2008, 2011; Davis
115 et al. 2014). It is overlain by the intermediate to felsic volcanoclastic rocks of the <2721 Ma

(Leclerc et al. 2012) Blondeau Formation (2-3 km thick). Near its base, the Blondeau Formation is intruded by the three ultramafic to mafic sills of the ca. 2717 Ma Cummings Complex (Dimorth et al. 1983; Mortensen 1993; Bédard 2009). The Bordeleau Formation consists of volcanoclastic deposits, arenite and conglomerate (Moisan 1992). The youngest part of the Bordeleau Formation transitions into the overlying <2692 to <2704 Ma Opémisca Group (Duquette 1982, Leclerc et al. 2012, David et al. 2006), which consists primarily of sandstones, siltstones, and polygenic conglomerates (Mueller and Dimroth 1984, 1986). In the south of the study area, the <2707 Ma or older (David et al. 2006) Caopatina Formation, which consists of volcaniclastic and sedimentary rocks, overlies the Obatogamau Formation (Mueller and Dimroth 1984, 1987).

In the study area several large-volume intermediate to felsic tonalite-dominated plutons, i.e., tonalite-trondhjemite-granodiorite (TTG) and TT-diorite (TTD) suites are coeval with the Roy Group. These correspond to syn-volcanic intrusions (Percival and Krogh 1983, Mathieu et al. 2020). One of these is the 2718 ±2 Ma Chibougamau pluton (Krogh 1982), the intrusion of which induced doming of the regional tectonic fabric (Racicot et al. 1984). This TTD pluton is genetically related to Cu-Au magmatic-hydrothermal mineralisation (Mathieu and Racicot 2019; Pilote et al. 1995). To the south of the Chibougamau pluton, which occupies the core of the Chibougamau anticline, the Boisvert and La Dauversière plutons (TTG suites), as well as the Eau Jaune Complex (TTD suite), are aligned in the E-W direction along the axial trace of the La Dauversière anticline (Pitcher 1979; Castro 1986). It is possible that syn-volcanic magmatism focused along east-west-striking structures in the study area (Mathieu et al 2020). Large-volume syn-volcanic magmatism is followed by syn-tectonic magmatism that consists of smaller-volume intrusions coeval with the Opémisca Group. Examples of the latter are the Chevrillon pluton (granodiorite), dated at 2695±3 Ma (Gariepy and Allegre, 1985), the Muscocho pluton (granodiorite), dated at 2701.2 +1.7/-1.3

Ma (Mortensen 1993) and undated alkaline intrusions (e.g. Saussure syenite), which intrude the volcanic and sedimentary rocks of the Roy and Opémisca groups. Syn-tectonic intrusions were emplaced during or toward the end of regional deformation and cut steeply-dipping volcanic and sedimentary units (Huguet 2019).

The Chibougamau area was mostly deformed and metamorphosed by terrane imbrication during and prior to the syn-tectonic, syn-Opémisca Group (deformation events D1, D2 and D3), as well as during the Grenville orogeny (1100-970 Ma; Rivers et al. 1989; Baker 1980; Daigneault and Allard 1990). The first phase of deformation (D1) is characterized by N-S to NNW-striking open synforms without associated axial planar cleavage (Daigneault et al. 1990) and may be associated with syn-volcanic faults, valleys, and other heterogeneities in the volcanic landscape (Legault 2003). The second phase (D2) initiates at ca. 2700 Ma or before, and may have continued after 2695 Ma (Leclerc et al. 2017; Mathieu et al 2020). This phase is associated with peak greenschist facies metamorphism and generated the main structures in the study area, including the main east-west trending foliation and ductile-brittle faults, as well as large-scale, east-trending, open folds. The D3 deformation phase mostly induced oblique-slip movements along the D2 structures and may correspond to the waning stage of the main deformation event (D2). The last deformation phase (D4) occurred during the Proterozoic (1100-970 Ma) and is only predominant in the rocks near the Grenville Front where it mostly consists of NNE-SSW brittle and ductile-brittle faults. The folds and faults produced during the D2 regional deformation are expected to be prominent features on the geophysical data and are described in more detail. From north to south, the main structures are (Daigneault et al. 1990) (Figures 1B and 1C):

(i) The Waconichi syncline (WS) is occupied by sedimentary rocks of the Opémisca Group, which is bordered by the east-west-trending Barlow and Faribault faults (Mueller et al. 1984).

(ii) The Waconichi anticline (WTZ) is 1 km thick and consists of several steeply-sipping tectonic panels. The southern limit of the WTZ is the Faribault fault (Daigneault 1982; Daigneault and Allard 1983, 1984; Daigneault and Allard, 1990; Leclerc et al., 2017).

(iii) The Chibougamau syncline (CS) is overprinted by the Waconichi tectonic zone (WTZ) and consists of steeply-sipping tectonic panels. It is occupied by the Blondeau Formation and the Cummings Complex is bordered, to the south, by the Lac Sauvage fault.

(iv) The Chibougamau anticline (CA) trends essentially east-west and curves toward the northeast near the Grenville front. The core of the anticline is occupied by the Doré Lake Complex (volcanic cycle 1) and the Chibougamau pluton (volcanic cycle 2). These intrusions induced doming of the lava pile, a feature that was then tightened during the D2 deformation event (Gobeil and Racicot 1983).

(v) The Chapais structure (ChS) is a half-syncline occupied by sedimentary rocks of the Opémisca Group and bordered, to the south, by the Kapunapotagen fault (Charbonneau et al. 1983; Daigneault and Allard 1983, 1987).

(vi) The La Dauversière anticline (DA) is occupied by several intrusive complexes (see above). This open fold corresponds to an area where stratigraphic polarities invert from top to the north to top to the south.

(vii) The Druillettes syncline (DS) is occupied by sedimentary rocks of the Caopatina Formation and is bounded by the east-west striking Guercheville and Doda faults (Sharma et al. 1987; Daigneault 1996).

The Abitibi greenstone belt contains a large amount of E-W-striking faults. In the Chibougamau area, these structures have caused a repetition of the stratigraphic sequence (Daigneault and Allard 1987). Two of these structures are subvertical east-west-striking faults, which are mostly syn-D2 structures that were still active (or reactivated) by the D3 event, and that separate sedimentary rocks from older volcanic rocks. In the CS, the Kapunapotagen fault is a north-verging thrust fault (Daigneault and Allard 1984), whereas in the WTZ, the Faribault fault is a north verging thrust (Daigneault and Allard 1983, 1984, 1987).

The geological map (Figure 1A) is used to define the geological formations at the surface of our 2D model section. The subsurface geology is also defined by four published geological cross sections (two of which are shown on Figure 1B and 1C; Daigneault et al. 1990) and the other two are from gravity forward modelling in the Chapais area (Dion et al. 1992).

3. Potential-field data

The Chibougamau transect has a total length of 128 km with a general NE-SW orientation. There is a total of 570 measured gravity observations along the profile collected by the Metal Earth project in 2017. In addition, publicly available gravity observations collected by the Geological Survey of Canada (GSC gravity database, 2019) were assessed and combined with our new database to provide information over a large area. New gravity stations were located along roads or within walking distance of roads, using an average spacing between observations of ~300 m (Maleki, 2019). Theoretically, this will allow structures larger and deeper than about 600 m to be resolved. However, where the acquired data values show sharp variations when displayed on plotted profiles, an infill station was placed midway between the initial stations to more precisely define the sources (location, dip and depth). Furthermore, measurements with 300 m spacing were

acquired on small (900 m) traverses perpendicular to the main transect, when side road access allowed.

Quality control was performed on the compiled gravity dataset and standard gravity processing were applied to the data, a density value of 2.67 g/cm^3 was used when calculating the Bouguer anomaly. Then the terrain correction was applied to the data to produce the complete Bouguer anomaly used for the modelling discussed in the next sections. The complete Bouguer anomaly ranges from -87 to -34 mGal across the study area (Figure 2A). The lowest values are associated with the Chibougamau and Opémisca plutons, while mafic-ultramafic intrusions and volcanic belts are associated with higher values.

Total magnetic intensity (TMI) datasets were obtained from the Ministère de l'Énergie et Ressources Naturelles du Québec (MERN). The highest resolution aeromagnetic datasets with a 75 meter cell size were leveled and used to generate the residual total-magnetic-field compilation shown in Figure 2B. To the north of the Chibougamau pluton, mafic to intermediate metavolcanic rocks of the Bruneau Formation, and mafic/ultramafic intrusions of the Cummings Complex have the strongest magnetic intensity value. The Chibougamau, Verneuil, La Dauversiere plutons and Eau Jaune Complex exhibit weak magnetic intensity, while intermediate metavolcanic and sedimentary rocks have weak to moderately high magnetic intensity. Most SW- and SE-trending magnetic lineaments are associated with Proterozoic dykes that have a high magnetic intensity.

Different processing procedures (e.g. reduction to pole, vertical derivative, tilt angle, analytic signal amplitude) were applied to enhance the edges of magnetized bodies and near-surface lineaments in order to perform a qualitative geological interpretation. The objective of the magnetic interpretation was to better delineate geological boundaries and features (e.g. dykes,

faults, and lithological contacts) where there is a contrast in magnetic susceptibility. The reduced to pole (RTP) magnetic grid was used to generate the second-vertical-derivative map (Hood, 1965) that is shown in colour on Figure 2C and is overlaid with the grey-scale tilt-angle map (Miller and Singh, 1994). This composite map highlights magnetic/geological boundaries. The new geological interpretation of the magnetic data (Figure 2D) provides additional geological information in areas that are covered by swamps, lakes and till deposits. The linear discontinuities with low magnetic contrast are generally associated with major faults, while SE- and SW-trending mafic dykes are associated with linear, short wavelength magnetic anomalies. The magnetic map has been used to generate a simplified bedrock geology map (Maleki 2019) to use as a constraint for the inversion. In this map geological units with similar petrophysical properties have been grouped together (Figure 2D). Also, features interpreted as Proterozoic dykes on Figure 2D were added to our sections, as many of these were not evident on the geological map. Specifically, several N-S-striking dykes have been added in the southern part of the "South" model. The magnetic data also indicate that the location of the Doré Lake Complex, where the "CSouth" and "CNorth" models intersect (Figure 2B and Figure 4), differs from that shown on the geology map, so this should be checked on the ground if there is outcrop available.

4. Seismic data

Seismic data collected by the Metal Earth project across the Chibougamau area was intended to image structures from the near-surface to Moho depths which is 37-40 km in the Abitibi greenstone belt (Winarrdhi and Mereu 1997; Mereu 2000). The seismic survey was acquired with a source separation of 50 m and a receiver separation of 25 m. The details of the seismic data acquisition and processing are described in Naghizadeh et al. (2019). Overall, the processing workflow was focused on robust static corrections, detailed velocity analysis, minimal trace smoothing, and high-resolution imaging. In this paper we will use the pre-stack time migrated (PSTM) seismic section of Metal Earth's Chibougamau transect to guide our potential-field modelling effort.

Previous research undertaken for Lithoprobe acquired three seismic reflection profiles across the eastern part of the Superior craton (i.e. the Opatica subprovince, the Abitibi greenstone belt, and the Pontiac metasedimentary subprovince) to define the geometry of the crustal structure at depth (Calvert and Ludden, 1999). Line 48 is the closest Lithoprobe line to the Chibougamau's Metal Earth transect and is located ~300 km to the west, in the Matagami area. The interpreted seismic section (Calvert and Ludden 1999) shows shallow reflections that dip shallowly to the north that may be associated with northward under-thrusting or a subduction zone in the upper mantle below the Opatica plutonic gneiss belt (Benn et at., 1992; Sawyer and Benn, 1993). Calvert and Ludden (1999) interpreted the mid-crust Abitibi belt as being composed of metasedimentary and igneous rocks with some unknown affinity units, and the Opatica belt as mainly orthogneisses. To the west of these profiles, Mints (2017) proposed that a fragment of the middle and lower crust of the Superior craton was exhumed within the north-south-striking Kapuskasing thrust fault zone. The Kapuskasing zone consists of mafic, tonalitic, and metasedimentary gneisses of amphibolite metamorphosed in the conditions of the granulites facies (Percival et al. 1992).

A preliminary geological interpretation of the Chibougamau seismic data is performed on dip coherency enhanced seismic sections (Figure 3) generated using the curvelet transform (Candes et al. 2006). The vertical axis of seismic sections were converted from time to depth using an average velocity of 6000 m/s (Christensen and Mooney 1995). The unreflective near-surface zones labeled as A, B, C and D are mainly interpreted as granodioritic bodies (plutons) intruded into the volcanic rocks. Some of these intrusions (A and B) do not outcrop on surface. The approximately 7 km near-surface zone (primarily shown as green) has fewer reflections than the deeper zone labeled as "mid-crust" on the section. The transition from the greenstone rocks in the near-surface to the mid-crust is shown as the top of the hatched zone on Figure 3. Mints (2017) interpreted a feature similar to this as a decollement surface. There are some reflectors along this boundary that match with the synclines and anticlines documented in the Chibougamau area. A dimming of reflectors sometimes occurs where the seismic line bends and the assumptions implicit in the common-midpoint processing method are not satisfied. This could have a negative impact on the coherent imaging of reflections.

Within the mid-crust (Figure 3), below an approximate depth of 7 km, the seismic images are characterized by gently dipping reflections, also in agreement with Mints (2017). Below the mid-crust, a zone is labeled 'lower crust' on the interpreted section, following Cook et al. (2010). Within the mid-crust, reflective horizons dipping gently to the north are observed. The dips are generally slightly steeper at shallow depths and flatten near the lower boundary. Similar flattening observed by Calvert and Ludden (1999) at a boundary between the mid- and lower crust was interpreted as a lower crustal decollement.

Seismic features have been used to define the deeper parts of our 2D section, specifically the top of the mid crust and the approximate location of the plutons (A, B, C and D in Figure 3).

5. Petrophysical data

Changes in the density and magnetic susceptibility can reflect variations in the lithology, weathering, hydrothermal alteration (Morris et al, 2007) and metamorphic grade (Cisowski and Fuller 1987; Boroomand et al. 2015). For example, higher density values are generally associated with rocks that are (i) mafic as opposed to lower-density felsic rocks, (ii) least weathered and (iii) that have been metamorphosed to higher metamorphic grade and are thus more compacted (Telford et al. 1976).

Eshaghi et al. (2019) combined petrophysical measurements, collected by the Metal Earth project, with compiled measurements collected across the Superior Craton and undertook a systematic characterization at a regional scale. For the Chibougamau traverse, few outcrops were close to the ME gravity stations, and we only had three readings of physical properties. Thus, in this area, we use the values tabulated in Dion et al. (1992) based on surface and borehole samples in the nearby Chapais region (Table 1). We therefore assume that the density of the rocks of the Chapais region are similar to those of the Chibougamau region and that the magnetic susceptibility values compiled by Eshaghi et al. (2019) for rocks in the Superior craton can be used to constrain the physical properties of models in this study area.

Main conclusions drawn from these two petrophysical datasets are as follows. Younger dykes (diabase) are mafic units with a high magnetic and density values compared to the other units of the studied area. Plutonic bodies have low densities and a narrow range of density values. Sedimentary and metamorphic rocks also display relatively low-density values. However, volcanoclastic packages can show a wide range of density values. Also, felsic and intermediate igneous rocks, sedimentary rocks and metamorphic rocks generally show low magnetic susceptibility values (Table 1).

In the sections we constructed, the mean values of magnetic susceptibility and density were assigned to specific geological units and these values were then adjusted to be consistent with the potential-field data. These adjustments account for weathering, hydrothermal alteration, metamorphism, and they should not exceed the maximum and minimum values measured in the field. However, sometimes the magnetic susceptibility had to be increased or decreased outside the expected range. We felt that this was likely due to normal or reversed remanent magnetization (Telford et al. 1976), which magnetic susceptibility instruments cannot measure. We hypothesize that when we had to make the susceptibility significantly more than expected, there was normal remanent magnetization present and when the susceptibility was less than expected, the remanent magnetization was reversed.

6. Modelling

Geosoft GMSYS software was used to perform forward modelling of gravity and magnetic data. This software assumes that the profile is two-dimensional (2D), i.e. the profile is a straight line and the strike of the geology runs perpendicular to the profile and is unchanging for an infinite distance away from it. Because the 128 km Chibougamau seismic traverse is not straight, it has been broken into four straight profiles: the South, CSouth, CNorth and North profiles (Figure 4). These profiles have also been extended beyond the area covered by seismic data. This was to allow more distal data from the GSC databases to be used to resolve deep structures. In this way structures down to 7 km depth were resolved by modelling gravity and to some extent magnetic data. The geology is rarely unchanging away from the profile, so the software allows for a finite strike length on either side of the section to be specified (this is termed 2.5-D modelling or a 2.5D correction). In the case of the CSouth and North profiles, the geological and magnetic interpretation maps (Figures 1A and 2D) were used to set the strike

length, on either side of the profile, to 5 km. For the South and CNorth profiles, the strike length was set to 2 km due to the structure being oblique to the profile direction.

6.1. Modelling results

For each profile, the complete Bouguer anomaly (includes ME and public datasets) and the residual magnetic field were forward modelled by manually adjusting the shape and physical properties of different geological units in order to minimize the differences between the modelled and the observed data (Olaniyan et al. 2013; 2014). We found that no variation in the depth of the Moho or lower crust was required to explain the gravity or magnetic data: all potential-field variations could be explained with adjustments to the physical properties or geometry of material in the top 7 km. When making adjustments to the model, we tried to ensure that the geological, seismic and petrophysical constraints were respected. The final models, for each profile, are presented and discussed in detail in the following four sections.

6.1.1 Profile South results and discussion

Profile South is 103 km in length, and is orientated in a SW-NE direction and includes the southern part of the Chibougamau seismic transect (Figure 4). Figure 5D illustrates a part of the interpreted seismic section used as a constraint. In the south, the Caopatina Formation has a density of roughly 2.70 g/cm^3, so it exhibits a relative gravity low (-72 mGal) compared to surrounding rocks (Figure 5B). The Caopatina Formation forms a sedimentary basin bounded by east-west striking faults (Sharma et al. 1987). In the middle of this broad low, at kilometre 15 on the profile, there is a moderate gravity high (-64.4 mGal, 5 km wavelength) that occurs in an area where there is outcrop of underlying mafic volcanic rocks (Obatogamau Formation; 2.85—2.95 g/cm^3). From 18 to 28 km along the profile in the Druillettes syncline, the gravity response increases with an approximately linear trend. This could be interpreted as a thinning

of the syncline, but we interpreted an underlying deeper fractured zone in the Obatogamau Formation (basalt, gabbro, andesite) with a density of 2.79 g/cm^3, as this is consistent with truncations of units observed in the seismic section. If this source has a density higher than 2.79 g/cm^3 and closer to the density of the unfractured Obatogamau Formation the fractured zone would be wider, while a lower density value would lead to a narrower geometry. This fractured zone is also consistent with a deformation zone observed on the surface in the Druillettes syncline. Subtle inflections, with short wavelengths from 25 to 29 km on the gravity profile could indicate fracture zones at these locations. The gravity continues to gradually increase northward from 28-40 km, followed by a significant (4.5 mGal) decrease from 40-48 km, which is interpreted to be due to a deep tonalitic pluton body (2.75 g/cm^3). At surface, this pluton corresponds to a narrower 2 km wide tonalitic outcrop on the geological map from 42 to 44 km. This plutonic body coincides with a reflector-free zone on the seismic data and is located along the same east-west trend of several tonalite-dominated plutons (Mathieu et al. 2020) such as the Eau Jaune Complex (TTD suite), the La Dauversière Pluton (tonalite-granodiorite), and the Boisvert Pluton (tonalite-granodiorite), all of which outcrop within the La Dauversière anticline (Figure 4). On the part of the profile where the Bruneau Formation (light green in Figure 5C) is shown coming close to surface (but actually does not outcrop) there is a slope down in gravity. This occurs at a zone where there are no reflectors on the seismic data. However, there is an outcrop of granodiorite off the profile (~ 1 km to the NW), which may be connected with our deep feature and could explain the gravity reduction. Further to the north, there is another decrease in the gravity response, which is interpreted to be associated with two adjacent geological features. The first is the Chapais syncline, which outcrops at 62-67 km and is occupied by the low-density sedimentary rocks (2.66 g/cm^3) of the Opémisca group (orange colour on the section) that overly sills of the Cummings Complex intruded into the Blondeau Formation (2.92 g/cm^3). The Chapais syncline is bordered to the

388 south by the Kapunapotagen fault. The second geological feature to the north is the
389 Chibougamau anticline, located at 67-90 km in the section. This anticline includes the low-
390 density Chibougamau pluton (2.70 g/cm^3) composed of tonalite (2.76 g/cm^3) in the center of
391 the pluton and of denser diorite (density=2.93 g/cm^3; Dion et al. 1992) along its margins. These
392 different phases within the pluton are consistent with the geological observations of Mathieu
393 and Racicot (2019). The gradual increase in gravity response to the north of the pluton is
394 interpreted to be due to a decrease in the thickness of the Chibougamau pluton, and to the
395 abundance of the diorite phase along its margin. The gravity data is consistent with a thickness
396 of the northern portion of the Chibougamau pluton of about 1 km, whereas the southern portion
397 is thicker, has a subvertical contact, and could extend to about 7 km at depth. At the north-
398 eastern end of the South profile, the geology consists of the Chibougamau anticline and the
399 Doré Lake Complex, but the profile is semi-parallel to the anticlinal structure. Hence, the
400 geometry and physical properties selected for the model are not reliable, as the 2.5D
401 assumptions are not well satisfied. However, the high gravity values in this section are
402 consistent with dense rocks composed of the main lithologies (anorthosite, gabbro, pyroxenite)
403 of the layered Doré Lake Complex (3.00 g/cm^3; Dion et al. 1992). In some parts of the profile,
404 sharp drops in the gravity response can be explained by buried granophyre (2.61 g/cm^3; Dion
405 et al. 1992), which is the uppermost unit of the Doré Lake Complex.

406 The residual magnetic intensity data exhibits a relatively flat magnetic response across the
407 South profile. However, there are some short-wavelength anomalies in the Druillettes syncline
408 that are interpreted to be caused by mafic intrusions and diabase dykes, in agreement with the
409 magnetic map interpretations (Figure 2D). Between 58 and 67 km along the profile, the
410 Cummings Complex, and mafic intrusions which underlay the sedimentary rocks of the
411 Opémisca group have been interpreted as the source of some short-wavelength magnetic
412 anomalies. The highest magnetic response along the South profile belongs to two anomalies

(3.3 and 2 km wavelength) over the Doré Lake Complex in the north-eastern end of the profile, which are modelled as two subvertical mafic intrusions with high magnetic susceptibilities. Small changes in the shapes of these bodies could result in better agreement between the model and measured data, but the precise geometries of these magnetic bodies were not considered an important part of modelling the deep structure.

6.1.2 Profile CSouth results and discussion

Profile CSouth is 44 km in length with an approximate S-N orientation. The location of the profile has been selected to include constraints from part of the Chibougamau seismic transect between 45 and 66 km. Figure 6D illustrates a part of the interpreted seismic section that is used as a constraint. Starting from the south, Figure 6C shows mafic rocks of the Obatagamau and the Bruneau Formations (density roughly 2.8 g/cm^3), between 0 and 7.7 km, that exhibit a flat gravity response. To the north of the Kapunapotagen fault, a gradual decrease of the Bouguer anomaly is associated with the Opémisca group (density ca 2.66 g/cm^3), which is interpreted to overlie the Bruneau Formation to the south and further to the north it overlies the southern corner of the Chibougamau pluton. These lower density rocks correspond to a gradual decrease in gravity response. The lowest gravity response (-73.36 mGal) along the CSouth profile is interpreted to be due to tonalitic/dioritic rocks (2.65 g/cm^3) in the Chibougamau anticline, which is consistent with an area without reflectors in the seismic profile. The thickness of the Chibougamau pluton, at the centre of the Chibougamau anticline changes thickness at the 16 km mark on the profile. The portion to the north is about 800 m thick and overlies the Obatogamau Formation (2.95 g/cm^3), whereas the southern thicker portion could extend to about 8 km. Some short wavelength fluctuations in gravity data between 20.5 to 25.7 km are interpreted to be due to slight changes in the thickness of the Chibougamau pluton in the thinner northern part. The smooth gradual increase in the gravity response from 25.7 km to

27 km is interpreted to be due to the gradual thinning of the Chibougamau pluton, and to a relatively thin body of the Obatogamau Formation against the fault. Further to the north toward 29.5 km, there is a steeper increase in gravity data from -46.5 to -39 mGal, which is interpreted to be due to an increase in the thickness of the denser lithologies, such as the Obatogamau and the Bruneau Formations (2.95-3.00 g/cm^3) with the depth extent not exceeding 3600 m. The Chibougamau syncline is bounded by two east-west oriented faults (the Lac Sauvage fault to the south, and the Faribault fault to the north), with dominant lithologies of the Cummings Complex sills and an assemblage of Roy Group rocks (Bruneau and Obatogamau Formations), having densities between 2.78 and 3.00 g/cm^3. The Chibougamau syncline corresponds to broad and smooth gravity high (-40 mGal) with a moderate decrease over intermediate to felsic volcanoclastic sediments of the Blondeau Formation (density ca 2.78 g/cm^3). The far north of the profile shows a gradual smooth decrease towards the Waconichi tectonic zone with sedimentary rocks of the Bordeleau Formation and mafic intrusions of the Cummings Complex.

The residual magnetic intensity profile is moderately flat along the southern 30 km. There are some short wavelength anomalies on the northern flank of the Chibougamau anticline, which are modelled as mafic intrusions and dykes with higher magnetic susceptibilities than surrounding rocks. The highest magnetic response is recorded over the Cummings Complex and mafic intrusions with high magnetic susceptibilities in the Chibougamau syncline. The lower magnetic field values from ~32 km to the end of the profile, is interpreted to be due to sedimentary rocks in the Chibougamau syncline (Blondeau Formation), and in the Waconichi Anticline (Bordeleau Formation) with low magnetic susceptibilities.

6.1.3 Profile CNorth results and discussion

Profile CNorth has a total length of 54 km with a general orientation of SW-NE. Between 65 km and 96 km, Figure 7D illustrates a part of the interpreted seismic section that is used as a constraint. Starting from the SW there are two adjacent geological features along the first 6 km of the profile resulting in a steep and linear decrease in the gravity response. The first one is the Opémisca Group with a density value of roughly 2.66 g/cm^3, which is interpreted to structurally overlie the Chibougamau plutonic body. The second feature is the Chibougamau pluton, a tonalitic/dioritic intrusion (density 2.65 – 2.70 g/cm^3) which is here interpreted to extent to 9 km at depth with subvertical contacts. The moderate increase in gravity response from 6 to 22 km is interpreted to be due to the gradual decrease in thickness of the Chibougamau pluton, and denser diorite phases occurring on the border of it. There are some short-wavelength fluctuations in the gravity response along the thinner northern portion of the Chibougamau pluton, which are interpreted as firstly due to depth fluctuations of the contact between the plutonic body and the underlying mafic rocks of the Obatogamau Formation, and secondly due to some hidden mafic intrusions and mafic rocks of the Doré Lake Complex (inserted to explain two 2.5 and 2 km wavelength gravity anomalies). Crossing the Lac Sauvage fault further to the north is the southern limit of the Chibougamau syncline which is marked by an increase in thickness of an assemblage of Roy Group rocks (Bruneau and Obatogamau Formations) with a density of 2.9 to 3 g/cm^3. These result in a generally gradual increase in gravity response from 22 to 27.7 km. It should be mentioned that the sharp change in the thickness of the Roy group rocks is consistent with the seismic interpretations, but the profile is semi-parallel to the strike of geological structure, and the transect is crooked in this area. The crooked transect compromises the seismic processing and the semi-parallel traverse violates the 2.5D assumption in the potential-field modelling. The gradual increase in gravity response continues toward 32.7 km which is interpreted to be due to the mafic intrusive body with a

density value of roughly 3.2 g/cm^3 which outcrops on the surface. A slight low in the gravity data at 29.5 km is observed over a location where there is an outcrop of basalt and andesitic basalts of the Bruneau Formation (2.7 – 2.9 g/cm^3), which overlies the previously mentioned mafic intrusive body. About 2 km further to the north, the flatter gravity response is interpreted to be due to basaltic and andesitic rocks of the outcropping Bruneau Formation having similar densities. Between 34.5 to 45 km, the gravity profile is generally flat with some subtle low-amplitude anomalies. The increases are interpreted to be due to the pyroxenite, dunite, and peridotite rocks of the Cummings Complex (density 2.7 to 2.9 g/cm^3). These rocks outcrop at a number of locations on surface. The slight decreases are interpreted to be related to intermediate to felsic volcanoclastic sediments of the Blondeau Formation (2.76 g/cm^3) which also outcrop on surface. North of the Faribault fault, the gravity is reduced in the Waconichi tectonic zone as a consequence of the less dense sedimentary rocks of the Bordeleau Formation.

The residual magnetic intensity profile exhibited an overall moderate flat response along the first ~34 km (Figure 7A). At 8, 13 and 19 km there are some increases in magnetic response on the northern flank of the Chibougamau anticline, which are modelled as buried mafic intrusions and dykes with higher magnetic susceptibilities than surrounded rocks. These anomalies are consistent with interpreted magnetic lineaments in Figure 2D. An alternative source for these features is hidden mafic intrusions and mafic rocks of the Doré Lake Complex with high magnetic susceptibilities. The largest magnetic anomalies are recorded over the Cummings Complex and mafic intrusions with high magnetic susceptibilities in the Chibougamau syncline from 34 to 46.5 km. Within these magnetic highs, the local lows are associated with sedimentary rocks of the Blondeau Formation (low magnetic susceptibility). There is a drop in magnetic response from ~46.5 km to the end of the profile, which is interpreted to be due to two low magnetic susceptibility sedimentary rocks; one in the

Chibougamau syncline (Blondeau Formation), and the other in the Waconichi anticline (Bordeleau Formation) both with low magnetic susceptibilities.

6.1.4 Profile North results and discussion

Profile North is 66 km in length and runs from south to north. The northernmost 28 km section coincides with the northern part of the Chibougamau seismic transect (Figure 8D). The southernmost 6.5 km of Figure 8C is covered by mafic rocks of the Obatagamau and the Bruneau Formations (~2.8 g/cm^3), which exhibit a smooth gravity response with a slight decrease attributed to an increase in the thickness of the Blondeau sedimentary rocks (density 2.68 g/cm^3). Crossing the east trending, south dipping Kapunapotagen reverse fault, the Opémisca group (~2.66 g/cm^3) in contact with anorthosite and gabbro of the Doré Lake Complex (2.98 g/cm^3) below and to the north, results in a gradual increase in the gravity response to the north. The lowest gravity response (-74 mGal) compared to surrounding regions is interpreted to be due to tonalitic/dioritic rocks (2.65 g/cm^3) of the Chibougamau pluton which could extend to about 7.7 km with subvertical contacts. The northern portion of the Chibougamau pluton overlies the Obatogamau and Bruneau Formations (2.95-2.97 g/cm^3) so there is a gradual increase in gravity response from 18 km to 21 km along the profile. There is a flat part of the gravity profile with some short wavelength fluctuations from 21 to 30.3 km, which is interpreted as changes in the thickness of Roy group rocks. Further to the north, there is a subtle short-wavelength gravity high at 32.8 km and with amplitude -35.5 mGal, which is interpreted to be due to the Cummings Complex (2.9-3.05 g/cm^3) which is supported by a mapped outcrop in the Chibougamau syncline. The zone covered by Blondeau sediments from 32.8-34.8 km shows a slight decrease in the Bouguer anomaly values. At 45.3 km, there is a gradual decrease in the gravity response which is interpreted to be due two factors: 1) a decrease in the thickness of the denser lithologies, such as the Bruneau Formations (2.9-2.95 g/cm^3) with

535 vertical extension not exceeding 2.3 km, and 2) the occurrence of sedimentary rocks of the
536 Opémisca Group with lower density than surrounding mafic to intermediate metavolcanic
537 rocks in the Waconichi syncline. Further to the north, there is a gravity high from 43.1-44.3
538 km which is interpreted to be due to high density mafic intrusions in the Waconichi syncline.
539 At 50.1 km, gravity values start to decrease. Although there is an interpreted reverse movement
540 of the Barlow fault which results in an increase in the thickness of the denser lithologies in the
541 footwall (Obatogamau and Bruneau Formations; density 2.85-2.95 g/cm^3), the measured
542 gravity values decrease. This is likely the impact of the deep and less dense
543 tonalitic/granodioritic rocks of the Barlow pluton (2.69 g/cm^3) and the tonalitic gneiss rocks of
544 the Opatica plutonic belt (2.66 g/cm^3) which are located at the extreme end of the profile and
545 are interpreted to extend to great depth. We have placed high density Obatogamau Formation
546 below the Barlow pluton, but, as there is no field evidence other higher density rocks could be
547 used such as mafic cumulus rocks at the base of the intrusions.

548 The residual magnetic intensity data appear moderately flat along the first 29 km. There are
549 some short wavelength anomalies on both the northern and the southern flanks of the
550 Chibougamau anticline, which are modelled as mafic intrusions and dykes with higher
551 magnetic susceptibilities than surrounding rocks. The highest magnetic response is recorded
552 over the Cummings Complex and mafic intrusions with high magnetic susceptibility content
553 in the Chibougamau syncline. There is a drop in magnetic data from 33 to 42.2 km, which is
554 interpreted to be due to the two sedimentary packages; one in the Chibougamau syncline
555 (Blondeau Formation), and the other in the Waconichi anticline (Bordeleau Formation). There
556 is a strong magnetic anomaly from 42.7 to 44.4 km which is consistent with a mafic intrusive
557 body with a higher magnetic susceptibility than the surrounding sediments in the Waconichi
558 syncline.

559

7. Discussion and Conclusion

Because of the non-uniqueness of potential-field data, in this study, we used various datasets (i.e. surface geology, magnetic map interpretation, interpreted seismic sections and petrophysical measurements) to produce reliable sections that model the geometry of geological features at depth.

Our primary emphasis was on the gravity data, which was used to resolve the shape and geometry of several features, and especially plutonic bodies. This is significant, especially for the Chibougamau pluton that is associated with Cu-Au magmatic-hydrothermal mineralisation. The magnetic data was used to focus on narrow planar structures (dikes) associated with magnetic contrasts. The gravity and magnetic modelling provided insights as to the shape of the plutons in areas where there were no reflections in the seismic data. When reflections are evident subsurface structures can be interpreted with more confidence.

In the La Dauversiere anticline (the South profile), a buried pluton was modelled at depth. This pluton potentially connects with an outcrop of granodiorite to the NW of the transect. Also, in the southern part of the South profile, in the Druillettes syncline, a fractured zone is interpreted in the Obatogamau Formation, which is relevant to the seismic interpretation and to the deformation zone observed at the surface.

Acknowledgement

The authors would like to thank Dr. Pierrick Altwegg, William McNeice, Fabiano Della Justina, Brandon Hume, Tara Smith, Kerri Campbell, and Pierre Bedeaux for their help during data collection, processing and interpretation. The authors acknowledge that the Metal Earth project, Harquail School of Earth Sciences, Laurentian University has provided a platform to perform this research. This work was supported by the Canada First Research Excellence Fund

584 (CFREF). The Metal Earth project would also like to acknowledge Seequent for providing four
585 Geosoft montaj licences, which allowed the processing of the magnetic and gravity data and
586 the GM-SYS modelling presented here. The contribution number of this publication is MERC-
587 ME-2019-225.

588 **References**

589 Allard, G.O. 1976. Doré Lake Complex and its importance to Chibougamau geology and
590 metallogeny. Ministère des Richesses Naturelles du Québec, DP 368.

591 Allard, G. O., and Gobeil, A. 1984. General geology of the Chibougamau region. In
592 Chibougamau-stratigraphy and mineralization. Edited by J. Guha and E. H. Chown. The
593 Canadian Institute of Mining and Metallurgy, Special Volume 34, pp. 5-20.

594 Baker, D. 1980. The metamorphic and structural history of the Grenville Front near
595 Chibougamau, Québec. Ph.D. thesis, University of Georgia, Athens, GA.

596 Bédard J.H., Leclerc F., Harris, L.B., Goulet, N., 2009. Intra-sill magmatic evolution in the
597 Cumming Complex, Abitibi greenstone belt: Tholeiitic to calc-alkaline magmatism recorded
598 in an Archean subvolcanic conduit system. Lithos 111, pp. 47–71.

599 Benn, K., Sawyer, E.W., and Bouchez, J.-L. 1992. Orogen parallel and transverse shearing in
600 the Opatica belt, Quebec: Implications for the structure of the Abitibi subprovince, Canadian
601 Journal of Earth Sciences, 29, pp. 2429-2444.

602 Boroomand, M.A., Safari, A., and Bahroudi, A., 2015. Magnetic susceptibility as a tool for
603 mineral exploration (Case Study: Southern of Zagros Mountains). International Journal of
604 Mining and Geo-Engineering, 49, pp. 57-66.

605 Caty, J.-L. 1975. Géologie de la demie ouest du canton de Richardson (comté d'Abitibi-
606 1065Est). MRN report DP 342, 2 maps; Ministère des Richesses Naturelles: Québec, QC,
607 1066Canada.

608 Calvert, A. J., and Ludden, J. N. 1999. Archean continental assembly in the southeastern
609 Superior Province of Canada. Journal Tectonics, 18, pp. 412-429.

610 Candes, E. J., L. Demanet, D. L. Donoho, and L. Ying, 2006. Fast discrete curvelet tranforms:
611 Multiscale Modeling and Simulation, 5, pp. 861-899. Castro, A. 1986. Structural pattern and
612 ascent model in the Central Estremadura batholith, Hercynian belt, Spain. Journal of Structural
613 Geology, 8, pp. 633-645.

614 Christensen, N. I. and Mooney, W. D., 1995. Seismic velocity structure and composition of the
615 continental crust: a global view: Journal of Geophysical Research, 100 (B6), pp. 9761-9788.
616 doi 10.1029/95JB00259Cisowski, S.M. and Fuller, M., 1987. The generation of magnetic
617 anomalies by combustion metamorphism of sedimentary rock, and its significance to
618 hydrocarbon exploration. GSA Bulletin 99, pp. 21-29.

619 Cook, F.A., White, D.J., Jones, A.G., Eaton, D.W.S., Hall, J., Clowes, R.M., 2010. How the
620 crust meets the mantle: lithoprobe perspectives on the Mohorovičić discontinuity and crust–
621 mantle transition. Canadian Journal of Earth Sciences, 47 (4), pp. 315–351.

622 Cooper, G. R. J., and D. R. Cowan, 2006. Enhancing potential field data using filters based on
623 the local phase: Computers & Geosciences, 32, pp. 1585-1591.

624 Daigneault, R. 1982. Demie nord du canton de McKenzie. Ministère de 1'Energie et des
625 Ressources du Québec, DP 82-08.

626 Daigneault, R., and Allard, G. O. 1983. Stratigraphie et structure de la région de Chibougamau.
627 In Statigraphie des ensembles volcanosédimetaires archéens de l'Abitibi: Etat des
628 connaissances. Ministère de 1'Energie et des Ressources du Québec, DV 83-13, pp. 1-18.

629 Daigneault, R., and Allard, G. O. 1984. Évolution tectonique d'une portion du sillon de roches
630 vertes de Chibougamau. In Chibougamau-stratigraphie and minéralisation. Edited by J. Guha
631 and E. H. Chown. The Canadian Institute of Mining and Metallurgy, Special volume 34, pp.
632 212- 228.

633 Daigneault, R., and Allard, G. O. 1987. Les cisaillements E-W et leur importance
634 stratigmphique et métallogénique, région de Chibougamau:In Études géoscientifiaues récentes.
635 Séminaire d'information 1987. Ministère de 1'Energie et des Resources du Québec, DV 87-25,
636 pp. 57-73.

637 Daigneault, R., & Allard, G. O. 1990. Le Complexe du lac Doré et son environnement
638 1095géologique (région de Chibougamau-sous-province de l'Abitibi). MRN report MM-
639 109689-03, Ministère des Ressources Naturelles: Québec, QC,Canada.

640 Daigneault, R., St-Julien, P., and Allard, G.O. 1990. Tectonic evolution of the northeast portion
641 of the Archean Abitibi greenstone belt, Chibougamau area, Quebec: Canadian Journal of Earth
642 Sciences, 27, pp. 1714–1736.

643 Daigneault, Réal. 1996. Couloirs de déformation de al Sous-Province de l'Abitibi. MRN report
644 MB-96-33, Ministère des Ressources Naturelles: Québec, QC, Canada.

645 David, J., Dion, C., Goutier, J., Roy, P., Bandyayera, D., Legault, M., & Rhéaume, P. 2006.
646 Datations U-Pb Effectuées dans la Sous-province de l'Abitibi à la suite des travaux de 2004-
647 2005. MRN report RP 2006-04 ; Ministère des Ressources Naturelles et de la Faune: Québec,
648 QC, Canada.

649 Davis, D., Simard, M., Hammouche, H., Bandyayera, D., Goutier, J., Pilote, P., et al. 2014.
650 Datations U-Pb Effectuées dans les Provinces du Supérieur et de Churchill en 2011-2012.
651 MERN report RP-2014-05; Ministère de l'Énergie et des Ressources Naturelles: Québec, QC,
652 Canada.

653 Dimorth, E., Muir, W., Rocheleau, M., Archer, P., Jutras, M., Piche, M., Simoneau, P.,
654 Carignan, J., Chown, E. H., Guha, J., Goulet, N., Allard, G. O., Franconi, A., and Gobeil, A.
655 1983. Stratigraphie et évolution du bassin de transition entre les Groupes de Roy et d'opémisca,
656 région de Chibougamau- Chapais. Stratigraphie des ensembles volcano-sédimentaires de
657 l'Abitibi : Etat des connaissances. Ministère de 1'Energie et des Ressources du Québec, DV 83-
658 1 1, pp. 21-35.

659 Dion, D.J., Morin, R., and Keating, P., 1992. Synthese geologique et geophysique de la region
660 de Chapais : portion orientale de la ceinture de I'Abitibi Quebecoise. Canadian Journal of Earth
661 Sciences, 29, pp. 314-327.

662 Duquette, G. 1982. Demie nord des cantons de McKenzie et de Roy et quart nord-ouest du
663 canton de McCorkill. MRN report DPV 837, 4 maps; Ministère des Ressources Naturelles:
664 Québec, QC, Canada.

665 Eshaghi, E., Smith, R. S., Ayer, J., 2019. Petrophysical characterisation (i.e. density and
666 magnetic susceptibility) of major rock units within the Abitibi Greenstone Belt. Laurentian
667 University Mineral Exploration Research Centre, publication number MERC-ME-2019-144.

668 Gariepy, C., and Allegre, C.J., 1985. The lead isotope geochemistry of late kinematic intrusives
669 from the Abitibi greenstone belt, and their implications for late Archean crustal evolution.
670 Geochimica and Cosmochimica Acta, 49, pp. 2371-2384.

671 Geosoft Inc., 2015. montaj gravity and terrain correction how-to Guide, available:
672 http://updates.geosoft.com/downloads/files/how- to guides/Gravity%20and%20Terrain%20
673 Corre -ction%20Formulas.pdf, [Date Accessed: 11th June 2015]

674 Gobeil, A., and Racicot, D. 1983. Carte lithostratigraphique de la région de Chibougamau au
675 11250 000. Ministère de 1'Energie et des Ressources du Québec, MM 83-02.

676 GSC (Geological Survey of Canada), 2019, The Canadian gravity anomaly database, accessed
677 at January 2019 at http://gdr.agg.nrcan.gc.ca/gdrdap/dap/search-eng.php

678 Henry, R. L., and Allard, G. 0. 1979. Formation ferrifère du Lac Sauvage, cantons de McKenzie
679 et de Roy, région de Chibougamau. Ministère des Richesses maturelles du Québec, DPV 593.

680 Hood, P. J., 1965, Gradient measurements in aeromagnetic surveying, Geophysics, 30, pp. 891-
681 902.

682 Hrouda, F. and Kapička, A., 1986. The effect of quartz on the magnetic anisotropy of quartzite.
683 Studia Geophysica et Geodaetica 30, pp. 39-45.

684 Huguet. J. 2019. Pétrographie et géochimie du Pluton de Chevrillon et relation structurale avec
685 le Groupe d'Opémisca (région de Chibougamau, Québec). Mémoire de maîtrise, Université du
686 Québec à Chicoutimi.

687 Kearey, P., Brooks, M. and Hill, I. 2012. An introduction to geophysics exploration; Blackwell
688 Science, Oxford, 268p.

689 Krogh, T. E. 1982. Improved accuracy of U-Pb zircon ages by the creation of more concordant
690 systems using air abrasion technique. Geochimica et Cosmochimica Acta, 46, pp. 637-649.

691 Leclerc, F., Bedard, J.H., Harris, L.B., Goulet, N., Houle, P., Roy, P. 2008. Nouvelles
692 subdivisions de la Formation de Gilman, Groupe de Roy, région de Chibougamau, Sous-

province de l'Abitibi, Québec: résultats préliminaires. Commission géologique du Canada; Recherches en cours 2008-7, 20 p.

Leclerc, F., Bedard, J.H., Harris, L.B., McNicoll, V., Goulet, N., Roy, P., Houle, P. 2011. Tholeiitic to calc-alkaline cyclic volcanism in the Roy Group, Chibougamau area, Abitibi Greenstone Belt, Revised stratigraphy and implications for VHMS exploration: Canadian Journal of Earth Sciences, 48, pp. 661-694.

Leclerc, F., Bédard, J.H., Harris, L.B., Goulet, N., Houle, P. and Roy, P. 2008. Nouvelles subdivisions de la Formation de Gilman, Groupe de Roy, région de Chibougamau, Sous-province de l'Abitibi, Québec : résultats préliminaires ; in Recherches en cours, Commission géologique du Canada, no. 2008-7, pp. 23.

Leclerc, F., Bédard, J.H., Harris, L.B., McNicoll, V.J., Goulet, N., Roy, P. and Houle, P. 2011. Tholeiitic to calcalkaline cyclic volcanism in the Roy Group, Chibougamau area, Abitibi Greenstone Belt–revised stratigraphy and implications for VHMS exploration; Canadian Journal of Earth Sciences, vol. 48, no. 3, pp. 661–694.

Leclerc, F., Harris, L. B., Bédard, J. H., van Breemen, O., & Goulet, N. 2012. Structural and Stratigraphic Controls on Magmatic, Volcanogenic, and Shear Zone-Hosted Mineralization in the Chapais-Chibougamau Mining Camp, Northeastern Abitibi, Canada. Economic Geology, 107(5), 963–989.

Leclerc, F., Roy, P., Houle, P., Pilote, P., Bédard, J.H., Harris, L.B., McNicoll, V.J., Van Breemen, O., Goulet, J.D. and Goulet, N. 2017. Géologie de la région de Chibougamau; Ministère de l'Énergie et des Ressources naturelles du Québec, RG2015-03, 97 p.

714 Legault, M. I. 2003. Environnement métallogénique du couloir de Fancamp avec emphase sur
715 les gisements aurifères de Chevrier, région de Chibougamau, Québec. Université du Québec à
716 Chicoutimi.

717 Ludden, J., Hynes, A. 2000. The Lithoprobe Abitibi–Grenville transect: two billion years of
718 crust formation and recycling in the Precambrian Shield of Canada: Canadian Journal of Earth
719 Sciences, 37, pp. 459-476.

720 Mathieu, L. 2019. Origin of the Vanadiferous Serpentine–Magnetite Rocks of the Mt. Sorcerer
721 Area, Lac Doré Layered Intrusion, Chibougamau, Québec. Geosciences, 9(3), 110.

722 Mathieu, L., and Racicot, D. 2019. Petrogenetic study of the multiphase Chibougamau pluton:
723 Archean magmas associated with Cu-Au magmato-hydrothermal systems. Minerals, 9,174.
724 35p.

725 Mathieu, L., Snyder, D.B., Bedeaux, P., Cheraghi, S., Lafrance, B., Thurston, Ph., and
726 Sherlock, R. 2020. Deep into the Chibougamau area, Abitibi greenstone belt: structure of a
727 Neoarchean crust revealed by seismic reflection profiling. Earth and Space Science Open
728 Archive, 58p.

729 Mathieu, L., Crépon, A., and Kontak, D.J. 2020. Tonalite-dominated magmatism in the Abitibi
730 Subprovince, Canada, and significance for Cu-Au magmatic-hydrothermal systems. Minerals,
731 10(3), 242

732 Maleki, A., 2019, Gravity data acquisition and potential-field data modelling along Metal
733 Earth's Chibougamau transect using geophysical and geological constraints. MSc thesis,
734 Laurentian University.

735 Mereu, R.F. 2000. The complexity of the crust and Moho under the southeastern Superior and
736 Grenville Provinces of the Canadian Shield from seismic wide-angle reflection data. Canadian
737 Journal of Earth Sciences. 37, pp. 439-458.

738 Miller, H. G., and Singh, V. 1994. Potential field tilt - a new concept for location of potential
739 field sources: Journal of Applied Geophysics, 32, pp. 213-217.

740 Mints, M.V. 2017. The composite North American Craton, Superior Province: Deep crustal
741 structure and mantle-plume model of Neoarchaean evolution. Precambrian Research 302, pp.
742 94–121.

743 Moisan, A. 1992. Pétrochimie des grès de la Formation de Bordeleau, Chibougamau Québec.
744 Unpublished Master thesis, Université du Québec à Chicoutimi.

745 Montsion, R., Thurston, P., and Ayer, J., 2018. 1:2 000 000 Scale Geological Compilation of
746 the Superior Craton – Version 1: Mineral Exploration Research Centre, Harquail School of
747 Earth Sciences, Laurentian University Document Number MERC-ME-2018-
748 017 https://merc.laurentian.ca/research/metal-earth/superior-compilation

749 Morris, W.A., Ugalde, H., and Clark, C., 2007. Physical Property Measurements: Boreholes
750 LB-07A, LB-08A, Lake Bosumtwi, Ghana. Meteoritics and Planetary Science 42, pp.801-811.

751 Mortensen, J. K. 1993. U - Pb geochronology of the eastern Abitibi subprovince. Part 1:
752 Chibougamau - Matagami - Joutel region. Canadian Journal of Earth Sciences, 30, pp. 11-28.

753 Mueller, W., and Dimroth, E. 1984. In Chibougamau, Stratigraphy and Mineralization, Edited
754 by J. Guha, E.H.Chown. Canadian Institute of Mining and Metallurgy, Special Volume 34, pp

755 Mueller, W., and Dimroth, E. 1987. A terrestrial-shallow marine transition in the Archean
756 Opemisca Group east of Chapais, Quebec. Precambrian Research, 37, pp. 29-55.

757 Muir, T.L. 2013. Ontario Precambrian bedrock magnetic susceptibility geodatabase for 2001
758 to 2012; Ontario Geological Survey, Miscellaneous Release—Data 273 – Revised.

759 Naghizadeh, M., Snyder, D., Cheraghi, S., Foster, S., Cilensek, S., Floreani, E., Mackie, J.,
760 2019. Acquisition and processing of wider bandwidth seismic data in crystalline crust: Progress
761 with the Metal Earth Project. Minerals 2019, 9, pp. 145-158.

762 Nowell, D.A.G. 1999. Gravity terrain corrections - an overview; Journal of Applied
763 Geophysics, 42, pp. 117-134.

764 Olaniyan, O.F., Smith, R.S., and Lafrance, B. 2014. A constrained potential field data
765 interpretation of the deep geometry of the Sudbury structure; Canadian Journal of Earth
766 Sciences, 51, pp. 715-729.

767 Olaniyan, O.F., Smith, R.S., and Morris, W.M. 2013. Qualitative geophysical interpretation of
768 the Sudbury Structure. Interpretation, 1, pp. 25-43.

769 Percival, J. A., and Krogh, T. E. 1983. U-Pb zircon geochronology of the Kapuskasing
770 structural zone and vicinity in the Chapleau- Foleyet area, Ontario. Canadian Journal of Earth
771 Sciences, 20, pp. 830-843.

772 Percival, J.A., Fountain, D.M., and Salisbury, M.H. 1992. Exposed crustal cross sections as
773 windows on the lower crust. in Continental Lower Crust. Edited by D.M. Fountain, R. Arculus,
774 and R.W. Kay. Elsevier, Amsterdam, pp. 317–362.

775 Pilkington, M., and P. Keating, 2010. Geologic application of magnetic data and using
776 enhancement for contact mapping: 2010 EGM International Workshop, Expanded Abstract.
777 pp. 1-5.

778 Pilote, P., Robert, F., Sinclair, W.D., Kirkham, R.V., and Daigneault, R., 1995, Porphyry-type
779 mineralization in the Doré Lake Complex: Clark Lake and Merrill Island area: Geological
780 Survey of Canada Open File 3143, pp. 65–86.

781 Pitcher, W. C. 1979. The nature, ascent and emplacement of granite magmas. Journal of the
782 Geological Society of London, 136, pp. 627-662.

783 Polat, A., Frei, R., Longstaffe, F.J., Woods, R., 2018. Petrogenetic and geodynamic origin of
784 the Neoarchean Doré Lake Complex, Abitibi subprovince, Superior Province, Canada.
785 International Journal of Earth Sciences 107, pp.811-843.

786 Racicot, D., Chown, E. H., and Hanel, T. 1984. Plutons of the Chibougamau-Desmaraisville
787 belt: a preliminary survey. In Chibougamau-stratigraphy and mineralization. Edited by J. Guha
788 and E. H. Chown. The Canadian Institute of Mining and Metallurgy, Special Volume 34, pp.
789 178-197.

790 Rivers, T., and Chown, E. H. 1986. The Grenville orogen in eastern Quebec and western
791 Labrador: Definition, identification, and tectonometamorphic relationships of autochtonous,
792 parautochthonous, and allochthonous terranes. In The Grenville Province. Edited by J. M.
793 Moore, A. Davidson, and A. J. Baer. Geological Association of Canada, Special Paper 31, pp.
794 31-50.

795 Rivers, T., Martignole, J., Gower, C., and Davidson, A. 1989. New tectonic divisions of the
796 Grenville Province, southeast Canadian Shield. Tectonics, 8, pp. 63-84.

797 Roest, W.R., Verhoef, J., and Pilkington, M. 1992, Magnetic interpretation using the 3-D
798 analytic signal, Geophysics, 57, pp.116-125.

799 Sawyer, E.W., and Benn, K. 1993. Structure of the high-grade Opatica Belt and adjacent low-
800 grade Abitibi subprovince, Canada: An Archaean mountain front, Journal of Structural
801 Geology, 15, pp. 1443-1458.

802 Scintrex Limited 2018. CG-6 AutogravTM gravity meter operation manual, https://
803 scintrexltd.com/wp-content/uploads/2018/04/ CG-6-Operations-Manual-RevB.pdf, 87p, [Date
804 Accessed: 2nd March 2018].

805 Sharma, K. M. N., Gobeil, A., and Mueller, W. l987. Stratigraphie de la région du Lac
806 Caopatina. Ministère de 1'Energie et des Ressources du Québec, MB 87-16.

807 Spector, A., and Grant, F.S. 1970. Statistical models for interpretating aeromagnetic data.
808 Geophysics, 35, pp. 293-302.

809 Telford, W.M., Geldart, L.P., Sheriff, R.E., and Keys, D.A., 1976, Applied Geophysics.
810 Cambridge University Press, 860p.

811 Telmat, H., Mareschal, J.C., Gariepy, C., David, J., and Antonuk, C.N. 2000. Crustal models
812 of the eastern Superior Province, Quebec, derived from new gravity data. Canadian Journal of
813 Earth Sciences, 37, pp. 385-397.

814 Winardhi, S., and Mereu, R.F. 1997. Crustal velocity structure of the Superior and Grenville
815 Provinces of the southeastern Canadian Shield. Canadian Journal of Earth Sciences, 34, pp.
816 1167–1184.

817 Wynne-Edwards, H. R. 1972. The Grenville Province. In Variations in tectonic styles in
818 Canada. Edited by R. A. Price and L. J. W. Douglas. Geological Association of Canada, Special
819 Paper II, pp. 263-334.

820 Yushkin, V. 2011. Operating experience with CG5 gravimeters; Measurement Techniques, 54.
821 pp.486-489.

822

823

824

825

826

827

828

829

830

831

832

833

834

835

836

837

838 Figure 1. Geological map of the Chibougamau area (A), showing the distribution of the folds
839 and faults mostly formed during the D2 regional deformation (modified after Montsion et al.
840 2018, Daigneault et al. 1990, Leclerc et al. 2008). The map was created using ArcGIS Desktop
841 version 10.5. The locations of two detailed cross-sections (A1-A5 and C1-C5) are denoted by
842 thick straight black lines. These sections are shown in (B and C) and are modified from
843 Daigneault et al. (1990).

844 Figure 2. Potential-field gravity and magnetic data of the Chibougamau area of interest. (A)
845 Complete Bouguer anomaly. (B) Total magnetic intensity. (C) Combination of 2nd vertical
846 derivative and tilt angle images. (D) Simplified geological interpretation of potential-field data
847 delineating physical property boundaries. The maps were created using ArcGIS Desktop
848 version 10.5 and Geosoft Oasis montaj version 9.7.

849 Figure 3. Interpretation of the Metal Earth Chibougamau curvelet-enhanced seismic transect.
850 The blue arrows on top illustrate parts which are relevant for the South, CSouth, CNorth, North
851 sections, which are four linear profiles which we have defined for the 2D modelling, the
852 locations of which are displayed in Figure 4.

853 Figure 4. The location of the modelled sections on the geological map. Legend as in Figure 1.
854 Modified after (Montsion et al. 2018, Daigneault et al. 1990, Leclerc et al. 2008). The map was
855 created using ArcGIS Desktop version 10.5.

856 Figure 5. The 2.5-dimensional geological model for profile South (C) and the corresponding
857 magnetic data and gravity data (A and B, respectively). The measured data is the thick dotted
858 line and the forward model data is the thin solid line. On the sections, the D label is associated
859 with the density (g/cm^3) and S denotes the susceptibility (SI). A part of the interpreted seismic
860 section was used as a constraint (D). Seismic constraints apply only between 12 - 56 km along
861 the profile. The top red arrows show the location of the intersection of the South and CSouth

862 profiles (#1), South and North profiles (#2). The blue upward arrows at the base of the section
863 show the locations of anticlines and synclines.

864 Figure 6. The 2.5-dimensional geological model for profile CSouth (C) and the corresponding
865 magnetic data and gravity data (A and B, respectively). The measured data is the thick dotted
866 line and the forward model data is the thin solid line. On the sections, the D label is associated
867 with the density (g/cm^3) and S denotes the susceptibility (SI). A part of the interpreted seismic
868 section was used as a constraint (D). Seismic constraints apply only from 3 – 24 km of the
869 profile. The top red arrows show the location of the intersection of the South and CSouth
870 profiles (#1), CNorth and CSouth profiles (#3). The blue upward arrows at the base of the
871 section show the locations of anticlines and synclines.

872 Figure 7. 2.5-dimensional geological model for profile CNorth (C) and the corresponding
873 magnetic and gravity (A and B, respectively) data from this study and GSC (2019) data. The
874 measured data is the thick dotted line and the forward model data is the thin solid line. On the
875 sections, the D label is associated with the density (g/cm^3) and S denotes the susceptibility (SI).
876 A part of the interpreted seismic section was used as a constraint (D). Seismic constraints apply
877 only from 17 – 48 km of the profile. The top red arrows show the location of the intersection
878 of the CNorth and CSouth profiles (#3), CNorth and North profiles (#4). The blue upward
879 arrows at the base of the section show the locations of anticlines and synclines.

880 Figure 8. 2.5-dimensional geological model for profile North (C) and the corresponding
881 magnetic and gravity (A and B, respectively) data from this study and GSC (2019) data. The
882 measured data is the thick dotted line and the forward model data is the thin solid line. On the
883 sections, the D label is associated with the density (g/cm^3) and S denotes the susceptibility (SI).
884 Seismic constraints (D) apply only from 37.5 – 65.5 km of the profile. The top red arrows show
885 the location of the intersection of the South and North profiles (#2), CNorth and North profiles

886 (#4). The blue upward arrows at the base of the section show the locations of anticlines and
887 synclines.

888 Table 1. Density and magnetic susceptibility measurements in Chapais area (Dion et al. 1992)
889
890
891
892
893
894
895
896
897

Lithology	N	Interval	Density (g/cm³) Average ± SD	Magnetic susceptibility (*10⁻³SI), interval
Opemisca Pluton				
Monzonite	6	2.62-2.64	2.63±0.008	0.01-0.8; 2.4-4.3
Presquile Pluton				
Tonalite	3	2.74-2.82	2.77±0.04	0.01; 0.2
Chibougamau Pluton				
Tonalite	12	2.60-2.73	2.67±0.04	0.01-2.3; 10-40
Diorite	21	2.73-3.06	2.93±0.1	0.01-2.3; 18-53
Opemisca Group				
Hauy Formation	10	2.72-2.97	2.87±0.07	0.1-0.5; 1.4-3.4
Stella Formation	4	2.71-2.76	2.74±0.02	0.1-0.5; 6.3-6.5
Daubree Formation	4	2.73-2.99	2.88±0.11	0.01; 0.6
cummings Complex				
Bourbeau Gabbro	9	2.83-3.05	2.97±0.07	0.01-0.6; 3-8
Ventures Gabbro	7	2.92-3.04	2.99±0.05	0.01-1.6; 12-45
Dunite	2	2.72-2.74	2.73	110; 190
Peridotite	6	2.66-2.79	2.73±0.04	72-130
Pyroxenite	5	3.12-3.27	3.21±0.06	0.8-8; 100
lac Dore Complex				
Anorthosite	2	2.99-3.00	2.99	0.01
Granophyre	1	2.61	2.61	0.2
Roy Group				
Blondeau Formation				
Sediments-tufs	24	2.66-2.91	2.79±0.06	0.01; 1.2
Andesite	8	2.75-2.83	2.79±0.04	0.01; 1.4
Gabbro dyke	6	2.85-2.98	2.90±0.05	17-100
Gilman Formation				
Basalt	11	2.80-3.23	2.99±0.13	0.01-1.6; 5-11
Gabbro	5	2.90-3.12	3.00±0.08	0.01-1.4; 6
Andesite	3	2.71-2.79	2.76±0.04	0.01; 0.4
Pyroclastic felsic	3	2.64-2.74	2.69±0.05	0.01; 0.1
Waconichi Formation				
Rhyolite	2	2.63-2.66	2.65	0.01; 0.1
Obatogamau Formation				
Basalt	27	2.73-3.10	2.95±0.12	0.01; 1.2
Gabbro	4	2.82-3.05	2.99±0.11	0.01; 1.4
Andesite	1	2.65	2.65	0.05
Chrissie Member	2	2.68-2.74	2.71	0.01; 0.5
Tonalitic Gneiss	22	2.56-2.77	2.67±0.05	---

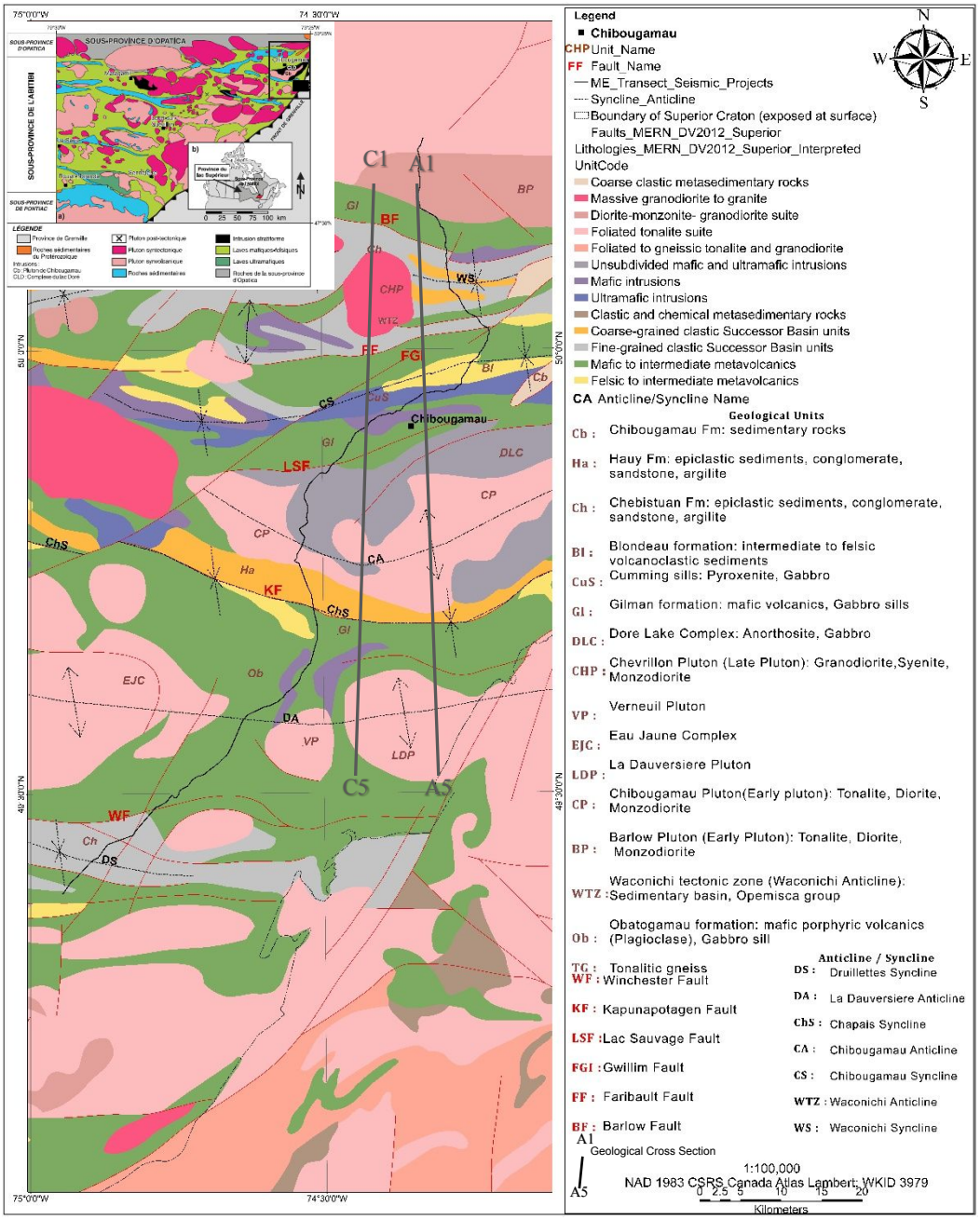

Figure 1.

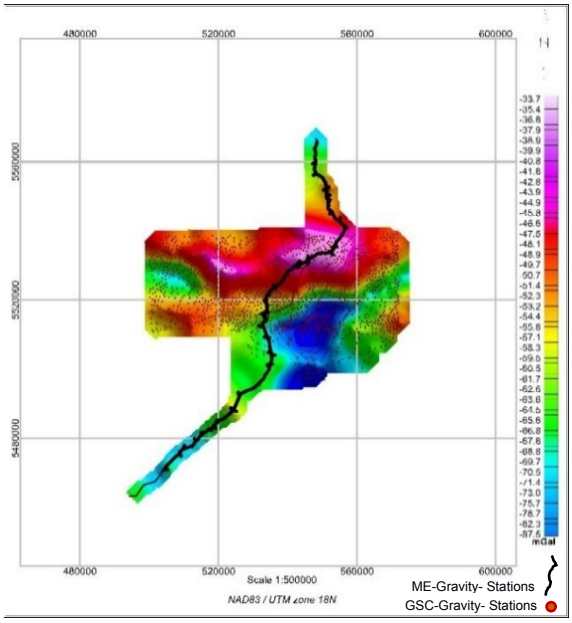

(A)

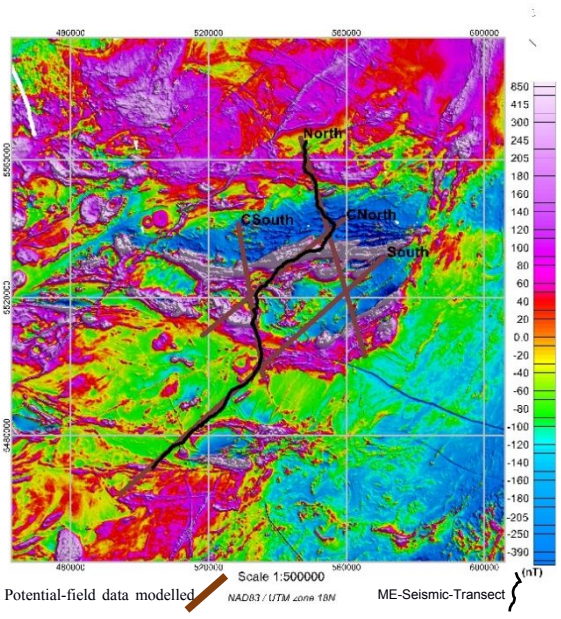

(B)

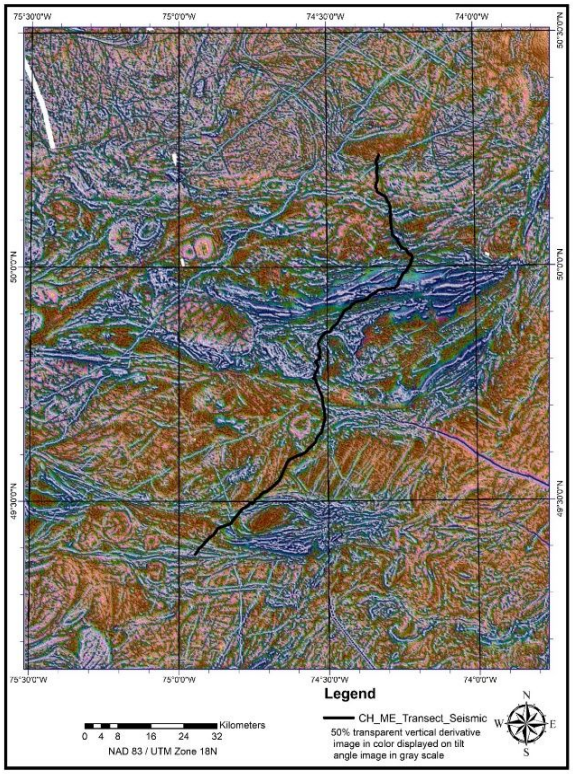

(C)

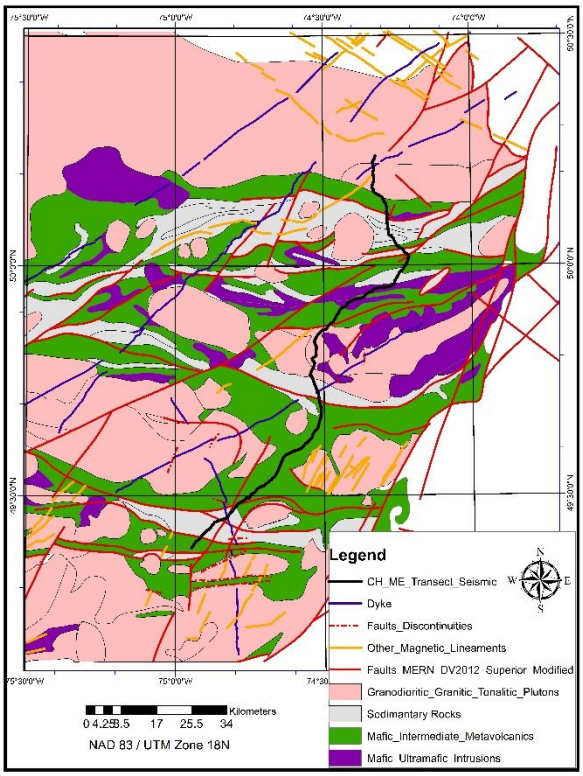

(D)

6

7 Figure 2.

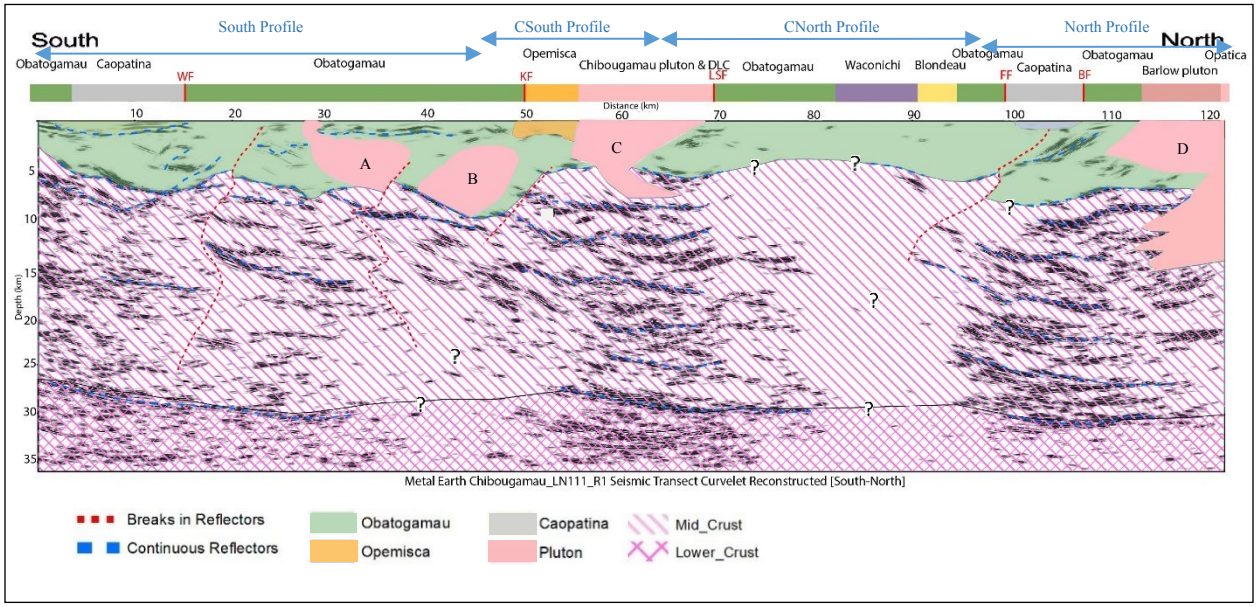

Figure 3.

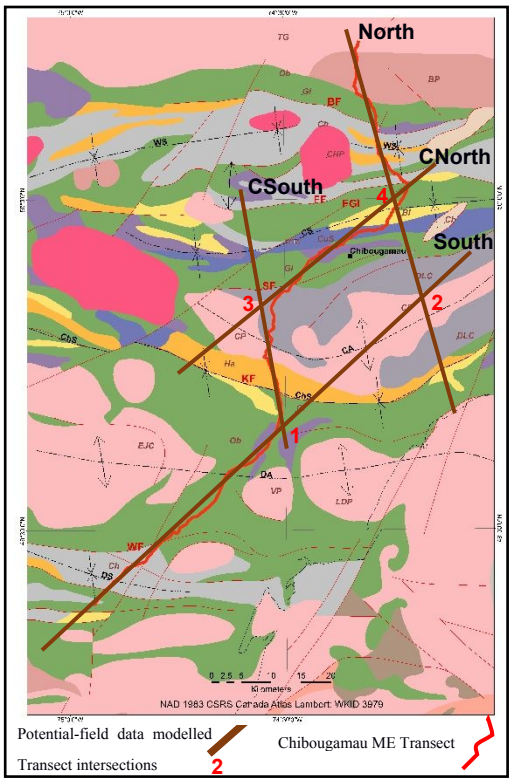

Figure 4.

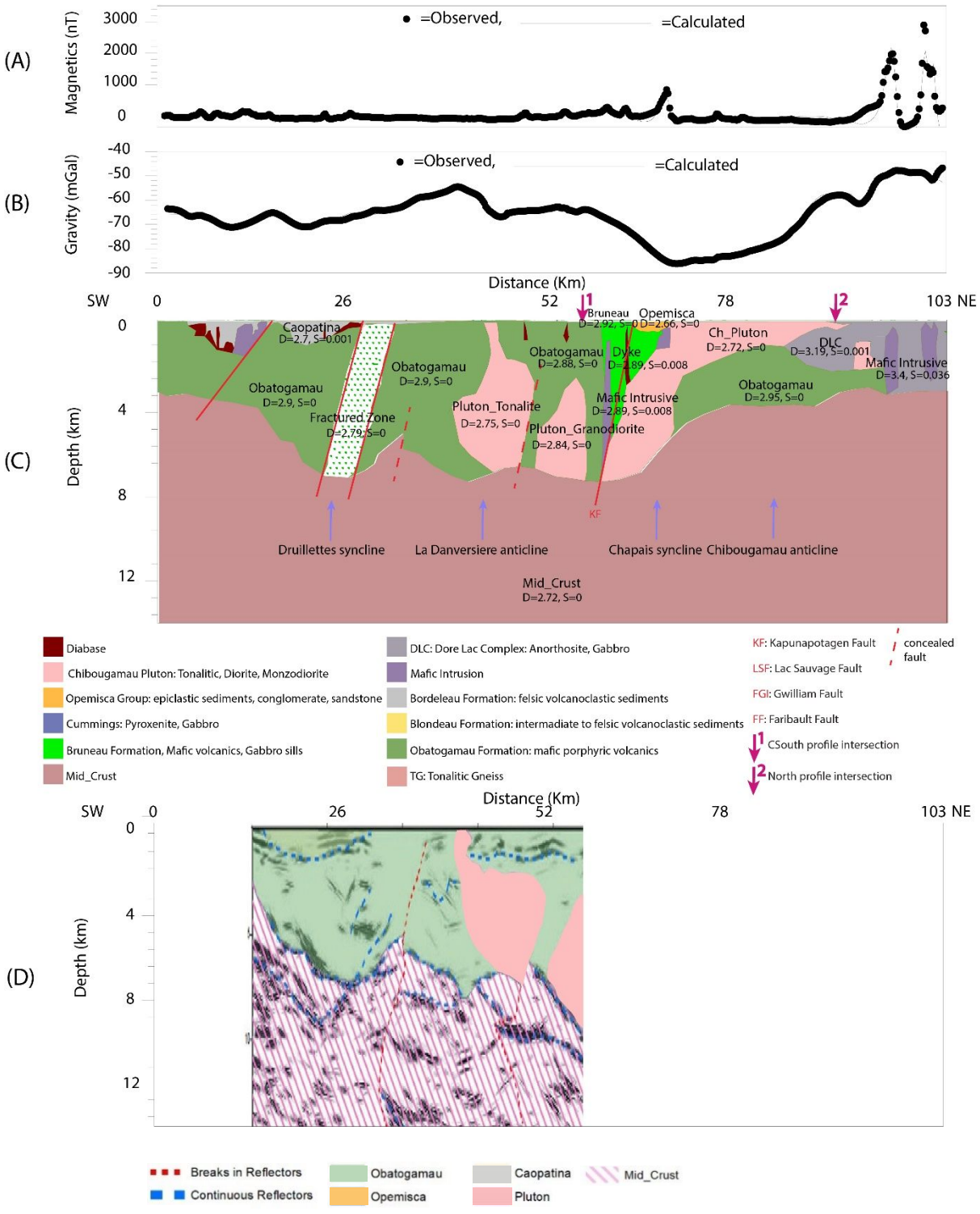

Figure 5.

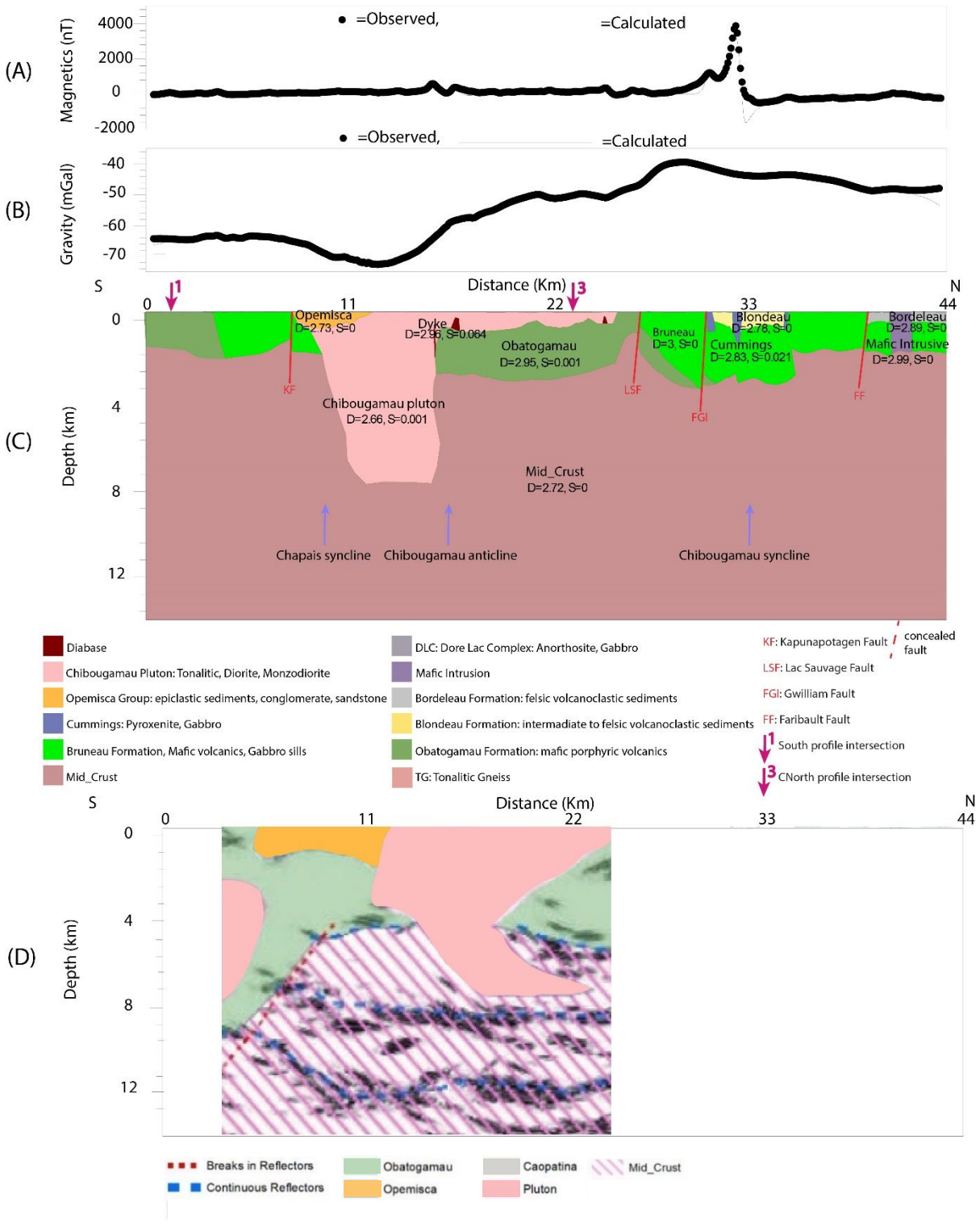

Figure 6.

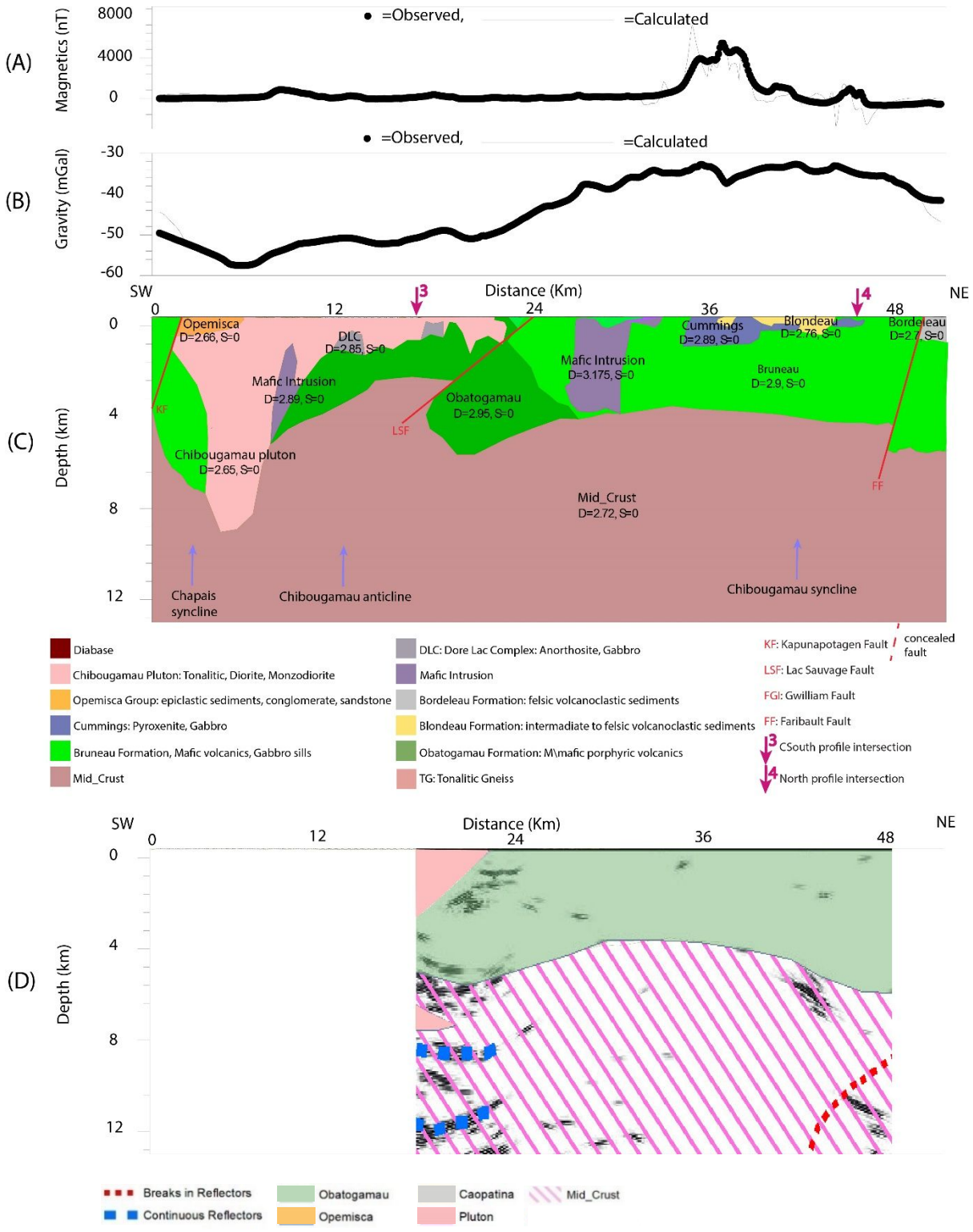

Figure 7

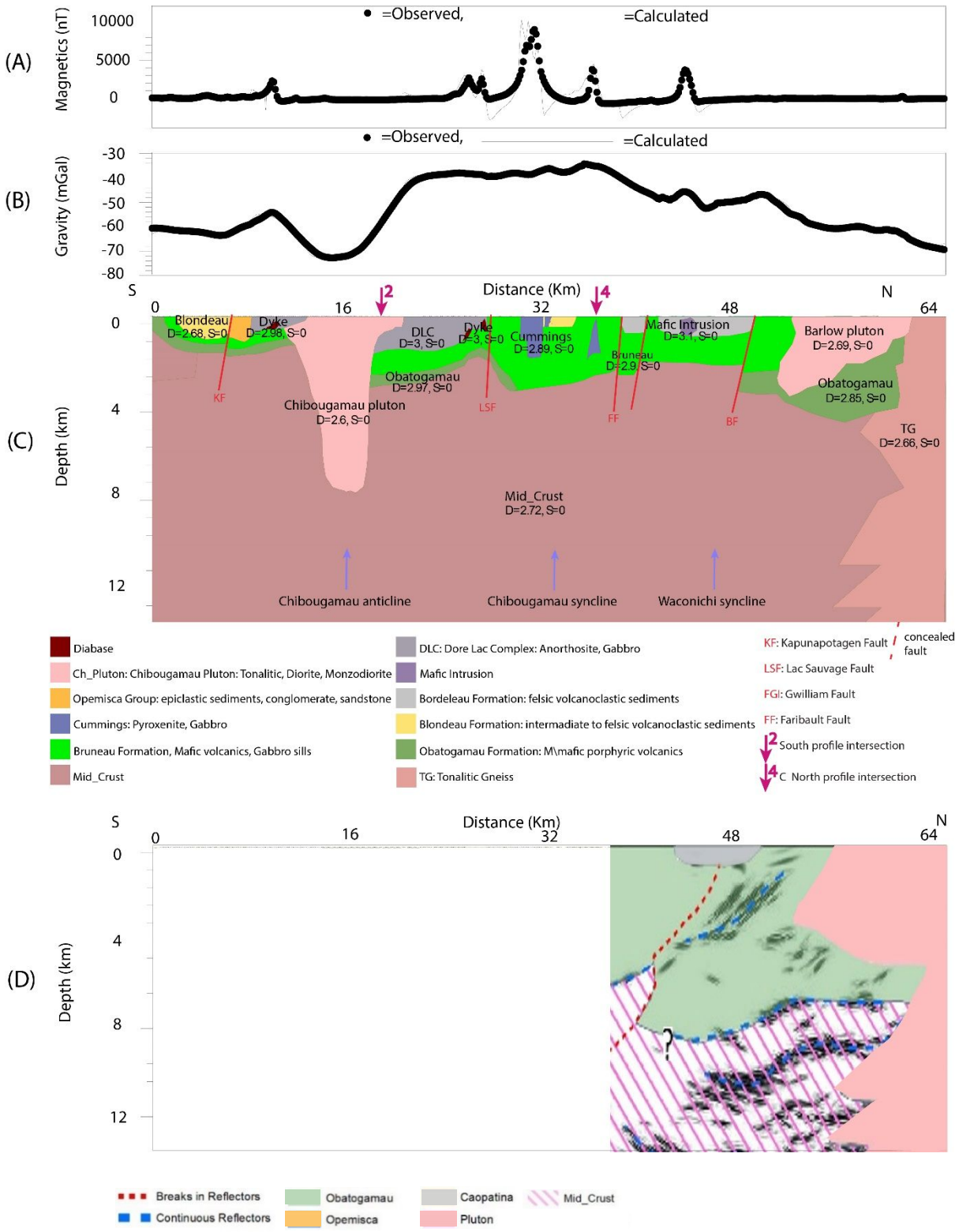

Figure 8